AGU PUBLICATIONS

JGR

Journal of Geophysical Research: Atmospheres

RESEARCH ARTICLE
10.1002/2015JD023470

Special Section:
Deep Convective Clouds and Chemistry 2012 Studies (DC3)

An improved lightning flash rate parameterization developed from Colorado DC3 thunderstorm data for use in cloud-resolving chemical transport models

B. M. Basarab[1], S. A. Rutledge[1], and B. R. Fuchs[1]

[1]Department of Atmospheric Science, Colorado State University, Fort Collins, Colorado, USA

Key Points:
- A 35 dB*Z* volume-based lightning parameterization predicts flash rate better than existing schemes
- Parameterizations based on updraft intensity were less successful than the 35 dB*Z* volume scheme
- The 35 dB*Z* volume scheme could be tested on larger data sets or implemented into models

Correspondence to:
B. M. Basarab,
bbasarab@atmos.colostate.edu

Citation:
Basarab, B. M., S. A. Rutledge, and B. R. Fuchs (2015), An improved lightning flash rate parameterization developed from Colorado DC3 thunderstorm data for use in cloud-resolving chemical transport models, *J. Geophys. Res. Atmos.*, *120*, doi:10.1002/2015JD023470.

Received 1 APR 2015
Accepted 12 AUG 2015
Accepted article online 14 AUG 2015

Abstract Accurate prediction of total lightning flash rate in thunderstorms is important to improve estimates of nitrogen oxides (NO_x) produced by lightning (LNO_x) from the storm scale to the global scale. In this study, flash rate parameterization schemes from the literature are evaluated against observed total flash rates for a sample of 11 Colorado thunderstorms, including nine storms from the Deep Convective Clouds and Chemistry (DC3) experiment in May-June 2012. Observed flash rates were determined using an automated algorithm that clusters very high frequency radiation sources emitted by electrical breakdown in clouds and detected by the northern Colorado lightning mapping array. Existing schemes were found to inadequately predict flash rates and were updated based on observed relationships between flash rate and simple storm parameters, yielding significant improvement. The most successful updated scheme predicts flash rate based on the radar-derived mixed-phase 35 dB*Z* echo volume. Parameterizations based on metrics for updraft intensity were also updated but were found to be less reliable predictors of flash rate for this sample of storms. The 35 dB*Z* volume scheme was tested on a data set containing radar reflectivity volume information for thousands of isolated convective cells in different regions of the U.S. This scheme predicted flash rates to within 5.8% of observed flash rates on average. These results encourage the application of this scheme to larger radar data sets and its possible implementation into cloud-resolving models.

1. Introduction

Thunderstorms impact their environment in a variety of ways, including the production of nitrogen oxides ($NO + NO_2 = NO_x$) by lightning. Recent observational and modeling research has sought to quantify the lightning NO_x (LNO_x) source across multiple scales and subsequent transport of NO_x to the upper troposphere (UT), where a local increase in NO_x can lead to net production of ozone (O_3), a potent greenhouse gas [*Liu et al.*, 1987; *Pickering et al.*, 1990, 1998; *Dye et al.*, 2000; *Fehr et al.*, 2004; *Schumann and Huntrieser*, 2007; *DeCaria et al.*, 2005; *Ott et al.*, 2010; *Cummings et al.*, 2013]. A potential increase in lightning in a warmer climate could drive a positive feedback to the warming as increased lightning NO_x production leads to more O_3 production in the UT [*Williams*, 1994; *Toumi et al.*, 1996]. Accurate estimates of LNO_x are therefore essential, but large uncertainty remains, with a commonly accepted best estimate for global LNO_x of 5 ± 3 Tg nitrogen mass per year [*Schumann and Huntrieser*, 2007]. Successful prediction of lightning flash rate across different spatial and temporal scales is a single yet crucial component in reducing LNO_x uncertainty in models.

Lightning flash rate is often estimated in cloud-resolving chemical transport models via flash rate *parameterization schemes*, meaning that flash rates are determined based on other predicted macroscopic storm quantities (storm parameters) known to relate to lightning flash rate, such as peak thunderstorm updraft speed [e.g., *Price and Rind*, 1992; *Pickering et al.*, 1998]. Lightning parameterizations are advantageous due to their low computational cost and large body of evidence demonstrating strong relationships between storm parameters and lightning [e.g., *Price and Rind*, 1992; *Deierling et al.*, 2005, 2008; *Deierling and Petersen*, 2008]. Prediction of lightning is essential not only in chemical transport models but also in general circulation models (GCMs) to understand lightning and its changes on a global scale [e.g., *Tost et al.*, 2007] and in operational models as a lightning forecasting aid [e.g., *McCaul et al.*, 2009]. A lightning parameterization should ideally be based on relatively simple storm parameters to be potentially applicable in a wide variety of model simulations.

A physically realistic lightning parameterization must implicitly consider the myriad microphysical and dynamical processes involved in the noninductive charging mechanism (NIC), thought to be the dominant mechanism responsible for thunderstorm electrification [*Saunders et al.*, 2006]. NIC is believed to occur primarily in the mixed-phase region of thunderstorms (defined herein as the region of cloud between the −5°C and −40°C isotherms), where rebounding collisions between riming ice hydrometeors (graupel) and small ice crystals in the presence of supercooled liquid water (SLW) result in a net transfer of charge [*Reynolds et al.*, 1957; *Takahashi*, 1978; *Jayaratne et al.*, 1983; *Saunders et al.*, 1991; *Williams et al.*, 1991]. Thunderstorm updrafts supply SLW to the mixed-phase region and loft the smaller charged ice crystals to high levels, while oppositely charged large graupel particles descend to lower levels, creating distinct charge regions between which strong electric fields can develop [*Reynolds et al.*, 1957]. Macroscopic indicators of updraft intensity, the amount of ice hydrometeors in the mixed-phase region of storms, and quantities related to the bulk separation of differently sized hydrometeors should therefore be indicative of the charging rate in thunderstorms and resulting frequency of lightning discharges [*Deierling and Petersen*, 2008; *Deierling et al.*, 2008].

Various past studies have indeed derived robust quantitative relationships between lightning flash rate and simple storm parameters representative of noninductive charging processes. *Price and Rind* [1992] derived lightning parameterizations relating flash rate to cloud-top height (a proxy for storm intensity) and to the peak thunderstorm updraft speed (W_{max}). For storms in northern Alabama and eastern Colorado, *Deierling and Petersen* [2008] found a strong correlation between total lightning flash rate and the volume of storm updraft exceeding 5 m s^{-1} at temperatures colder than −5°C (UV5, $r = 0.93$), while *Deierling* [2006] noted a comparably robust correlation between total lightning and updraft volume greater than 10 m s^{-1} (UV10). *Deierling and Petersen* [2008] also found a somewhat weaker correlation between lightning flash rate and W_{max} ($r = 0.82$). *Deierling et al.* [2008] developed empirical relationships between flash rate and dual-polarization radar-derived precipitating ice mass (graupel and hail, referred to herein as PIM) as well as the product of the upward flux of nonprecipitating ice (ice crystals and aggregates) and the downward flux of precipitating ice (P_{flux}). The PIM and P_{flux} parameters were strongly correlated to flash rate ($r = 0.94$ and $r = 0.96$, respectively). The volume of graupel in the mixed-phase region (GEV, a quantity similar to PIM) has been shown by past studies to be related to lightning activity for individual storms [e.g., *Carey and Rutledge*, 1996; *Wiens et al.*, 2005]. The mixed-phase volume of radar reflectivity greater than 35 dB*Z* (VOL35) was found by *Liu et al.* [2012] to be well correlated to lightning activity for radar precipitation features identified in the Tropical Rainfall Measuring Mission data set (correlation coefficient of 0.86). Prediction of lightning based on proxies for noninductive charging processes has also shown promise on the global scale. *Finney et al.* [2014] used reanalysis data to develop a parameterization based on upward cloud ice mass flux in the midtroposphere (440 hPa). This parameterization predicted global lightning in closer agreement to observations than several existing schemes, including the *Price and Rind* [1992] cloud-top height scheme. *Barthe et al.* [2010] tested a number of flash rate parameterizations from the literature in cloud-resolving model simulations of a single cell thunderstorm in Alabama and a severe storm in Colorado. Their study found variable results: some schemes predicted flash rates well for one storm but not the other, possibly suggesting a regional limitation on the application of certain flash rate schemes.

This study aims to evaluate and update existing lightning flash rate parameterizations based on a sample of Colorado thunderstorms observed during the Deep Convective Clouds and Chemistry (DC3) field project in May-June 2012 [*Barth et al.*, 2014] and during an in-house field project during summer 2013 (section 2). DC3 documented the microphysical and dynamical properties, transport of chemical species, and lightning NO_x production of thunderstorms in northeastern Colorado, central Oklahoma, and northern Alabama. High-resolution lightning mapping array (LMA) observations in each DC3 domain provided the means to estimate total (intracloud plus cloud-to-ground) lightning flash rates and to map individual flash locations and sizes via detection of very high frequency (VHF) radiation (60–66 MHz) emitted during electrical breakdown [*Rison et al.*, 1999]. The use of dual-polarization radars and multiple-Doppler radar networks during DC3 facilitated the comparison between flash rates and radar-derived bulk storm quantities, such as storm ice mass and updraft characteristics. Five schemes from the literature are evaluated herein, including the *Price and Rind* [1992] W_{max} and cloud-top height schemes (referred to as PR92W and PR92CTH), the *Deierling and Petersen* [2008] UV5 scheme (DP08), and the *Deierling et al.* [2008] PIM and P_{flux} schemes (D08P and D08F).

There exists large variability in thunderstorm total flash rates across the DC3 observational domains, likely due to the accompanying regional variability of environmental thermodynamic parameters hypothesized to influence flash rate such as warm cloud depth (WCD, defined herein as the vertical distance between the

lifting condensation level and the environmental 0°C isotherm), cloud base height, and the vertical distribution of convective available potential energy (CAPE) [e.g., *Williams et al.*, 2005; *Fuchs et al.*, 2015a]. *Fuchs et al.* [2015a] found high flash rates to be linked to large values of normalized convective available potential energy (NCAPE), where NCAPE is equal to CAPE divided by the height difference between the equilibrium level and the level of free convection, i.e., the CAPE depth [*Blanchard*, 1998]. Large NCAPE is thought to enhance noninductive charging by promoting stronger updrafts at low levels and increased lofting of SLW into the mixed-phase region. High flash rate storms accompanied by large NCAPE were more common in Colorado than in other regions, such as Alabama. *Fuchs et al.* [2015a] also found high flash rates to be linked to shallower WCDs, presumably because a shallow warm cloud layer diminishes warm rain collision-coalescence processes, allowing increased amounts of condensed water to ascend into the mixed-phase region. It is uncertain whether lightning parameterizations developed for storms in the semiarid region of Colorado are applicable to storms in different environments with typically different flash rates. This study therefore addresses the following questions, focusing on lightning parameterizations tailored to predict flash rates for the selected Colorado storms:

1. Do relationships between lightning flash rate and simple bulk storm parameters from the literature, or modified relationships derived from the Colorado data set analyzed herein, reliably predict lightning activity in the sampled Colorado thunderstorms?
2. Are flash rate parameterizations developed for a single region (Colorado) applicable to storms in other regions (e.g., Alabama) with different thermodynamic environments? With the advent of satellite-based radar observing platforms with near global coverage [e.g., the Global Precipitation Measurement (GPM) mission, *Smith et al.*, 2007], what are the implications for applying a radar-based lightning parameterization on a much larger scale?

Question 1 is important to ultimately reduce uncertainty in prediction of LNO_x produced by individual thunderstorms. Section 2 of this work focuses on the methods used to calculate storm parameters and total lightning flash rates. Section 3 presents the results of testing existing and modified flash rate parameterizations against observations of flash rates in the selected Colorado thunderstorms. In section 4, we analyze the performance of a selected flash rate parameterization for a larger data set of storms and as a function of a thunderstorm's environment, to answer question 2. A summary and recommendations for future work are provided in section 5.

2. Data and Methods

To examine relationships between lightning and storm parameters, gridded polarimetric radar observations and three-dimensional wind retrievals were merged with LMA data for 11 storms in northeastern Colorado. These Colorado data included 183 storm volume scans (183 total data points); dual-Doppler wind retrievals were possible for seven of the 11 Colorado cases for a total of 96 volume scans. Nine of the 11 Colorado cases were documented during the DC3 observational period (May-June 2012), and two were observed during summer 2013 during the CHILL Microphysical Investigation of Electrification (CHILL-MIE) in-house field project [*Fuchs et al.*, 2015b]. A map of the Colorado DC3 experimental design, including the location of the radars used in this study and the stations comprising the Colorado LMA network, is provided in Figure 1.

2.1. Radar Data

This study makes use of radar volume scans consisting of multiple radar sweeps at ascending elevation angles through a constant azimuth range. During the DC3 field project, the primary radars employed in the Colorado domain were the Colorado State University (CSU)-CHILL S-band dual-polarization Doppler radar located in Greeley, CO, and the CSU-Pawnee S-band Doppler radar, located about 50 km to the north-northwest. The CHILL and Pawnee radars were used for all dual-Doppler wind retrievals in this study, and CHILL was used for all polarimetric retrievals during DC3. During DC3 and CHILL-MIE, CHILL operated in alternating horizontal and vertical transmit modes to retrieve radar reflectivity (Z), radial velocity (VR), spectrum width (SW), differential reflectivity (Z_{DR}) [*Seliga and Bringi*, 1976], propagation differential phase (ϕ_{DP}) [*Hubbert and Bringi*, 1995], correlation coefficient (ρ_{HV}) [*Balakrishnan and Zrnic*, 1990], and linear depolarization ratio (LDR) [*Bringi and Chandrasekar*, 2001]. Polarimetric retrievals were also obtained for one CHILL-MIE case from the National Weather Service (NWS) Weather Surveillance Radar 1988-Doppler Polarimetric (WSR-88DP) radars in Cheyenne, WY (KCYS), and near Denver, CO (KFTG).

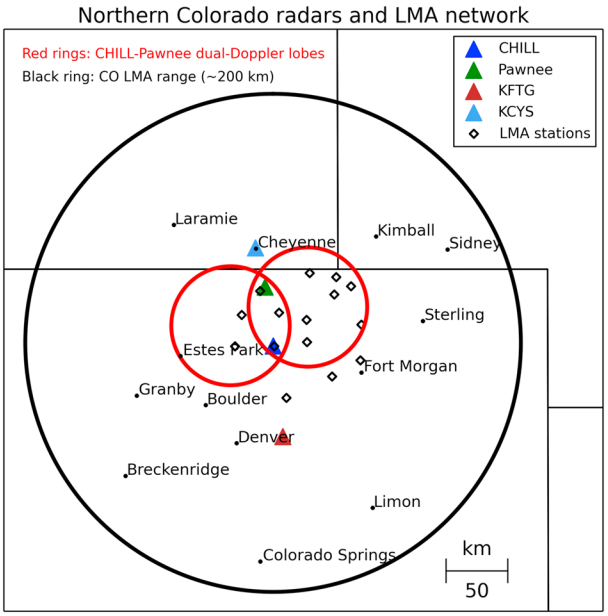

Figure 1. Map of the Colorado DC3 experimental design showing the locations of the four radars used in this study (colored triangles), the CHILL-Pawnee dual-Doppler lobes (red circles), the location of stations comprising the northern Colorado LMA network (black diamonds), and a range ring of radius 200 km (black circle) depicting the approximate range from the LMA center over which lightning flashes are reliably detected. Locations of various cities and towns in the surrounding region are also indicated for spatial reference.

The radar data were first inspected manually, and any aliased velocity fields were corrected using the National Center for Atmospheric Research (NCAR) solo3 software [*Oye et al.*, 1995, https://www.eol.ucar.edu/software/solo3]. The specific differential phase (K_{DP}) [*Hubbert and Bringi*, 1995] was calculated from the ϕ_{DP} field using the method of *Wang and Chandrasekar* [2009]. For CHILL data, all polarimetric fields and particle fall speeds (estimated from the hydrometeor identification output, see section 2.2) were gridded using the NCAR Sorted Position Radar INTerpolation software [*Mohr and Vaughan*, 1979; *Miller et al.*, 1986]. WSR-88DP data were gridded using the NCAR REORDER software package [*Oye and Case*, 1995]. All radar data were gridded to 0.5 km resolution in the horizontal and vertical. Radar data fields were automatically thresholded on a flag designed to indicate regions of noise and nonmeteorological targets such as range-aliased echo and ground clutter. This flag was created based on values of the normalized coherent power (NC). The data were manually inspected after applying this automated threshold, and it was confirmed that nonmeteorological echoes had been adequately removed.

2.2. Hydrometeor Identification

In order to calculate storm ice content and relate storm microphysical properties to the wind fields, gridded polarimetric radar variables were used to determine the dominant hydrometeor types within storms. For all sampled storms, polarimetric radar retrievals combined with temperature data from NWS soundings closest to the storms were input to a fuzzy logic hydrometeor identification algorithm (HID) developed by *Dolan et al.* [2013]. The HID outputs 10 hydrometeor categories: drizzle, rain, ice crystals, aggregates, wet snow, vertically oriented ice crystals, low-density graupel, high-density graupel, hail, and big drops (defined as drops with diameters exceeding 5 mm). The HID is based on a series of membership beta functions (MBFs), developed from electromagnetic scattering simulations of each polarimetric variable assuming size, shape, and density distributions for each hydrometeor category as a function of temperature [*Dolan and Rutledge*, 2009]. MBFs range from zero to one and indicate the probability at each grid point that a certain hydrometeor type exists for the observed values of the polarimetric variables. The values of all MBFs were then weighted and summed for each hydrometeor type to arrive at a score for that type. The hydrometeor type with the highest score at a grid point was determined to be the dominant category. Inspection of the HID output for several cases (not shown) demonstrated that the dominant hydrometeor type typically scored much higher than any other type, evidence that the assumption of a dominant hydrometeor category at each grid point was generally valid for the purpose of calculating bulk storm ice mass quantities.

2.3. Retrieval of Three-Dimensional Wind Fields

In order to measure storm updraft intensity, the three-dimensional wind field was synthesized from gridded radial velocity data. Since radial velocity fields can contain a contribution from particle fall speeds, particle fall speeds were calculated at each grid point and incorporated into the analysis. Estimates of particle fall speeds were determined by reducing the 10-category HID (section 2.2) to four simpler categories: rain, graupel/hail, dry snow, and wet snow. Separate reflectivity-fall speed relationships for these four categories from *Giangrande et al.* [2013] were assumed.

Gridded radial velocity fields from the CHILL and Pawnee radars and particle fall speed fields were read into the Custom Editing and Display of Reduced Information in Cartesian Space software [*Mohr et al.*, 1986]. First, the particle fall speed estimates were used to generate linear equations relating the three Cartesian components of the wind field (u, v, and w) to the observed radial velocities at each point on the Cartesian grid. At each point, w was initially set to zero so that u and v could be explicitly calculated. Then the horizontal divergence was computed, allowing an initial estimate of w to be obtained by integration of the anelastic mass continuity equation,

$$\frac{\partial u}{\partial x} + \frac{\partial v}{\partial y} + \frac{\partial w}{\partial z} = -\frac{w}{\rho_0}\frac{\partial \rho_0}{\partial z} \tag{1}$$

where air density ρ_0 is assumed to vary with z only [e.g., equation (4) of *Ray et al.*, 1980]. A downward integration method was used, which assumes a boundary condition of $w = 0$ at the top of the radar domain, defined as a radar reflectivity of 0 dBZ. The resulting w field was used to recompute u and v from the system of linear equations, and the process was repeated iteratively until solutions for u and v converged, a common solution method outlined by *Ray et al.* [1980]. From the final iterative solutions for u and v, the horizontal divergence was calculated and integrated to obtain a final solution for w. This dual-Doppler method has been shown to result in relatively small errors in w, on the order of 5 m s^{-1}, in strong updraft cores [e.g., *Calhoun et al.*, 2013].

2.4. Objective Identification of Storms

To accurately calculate storm parameters and attribute detected lightning flashes to individual storms, reflectivity regions corresponding to storm cells were objectively identified using the Colorado State University (CSU) Lightning, Environmental, Aerosol, and Radar (CLEAR) framework developed by *Lang and Rutledge* [2011] and *Fuchs et al.* [2015a]. The CLEAR framework ingests large amounts of data of various types and attributes those data to features of interest identified and tracked by the software. In this way, quantitative relationships between storm parameters and flash rates can be analyzed. CLEAR was shown by *Fuchs et al.* [2015a] to consistently and successfully track isolated convective storm cells. That study gives a more detailed description of CLEAR and its capabilities. In the present work, the CLEAR tracking algorithm was used to identify individual storm cell areas as contiguous regions of composite reflectivity and assign those cells to a particular storm track. The cell and its characteristics represent the storm at one particular time, and the track contains cell information over the entire lifetime of a storm. The CLEAR software retains information about the motion of previously identified tracks to determine whether a new cell should be part of an existing track or become a new track.

Potential cells were initially identified based on contiguous 35 dBZ composite reflectivity regions that exceeded a specified area threshold. This 35 dBZ threshold was chosen so that identified cells were likely convective in nature and electrified. Within an identified 35 dBZ cell area, a higher, "second-tier" contiguous composite reflectivity region was then examined, which for most cases was the composite reflectivity region exceeding 45 dBZ. Similar reflectivity thresholds have been used by past studies to identify and track isolated convective cells [e.g., *Rowe et al.*, 2011]. For some weaker storms, a lower second-tier reflectivity threshold was used so that these storms could be tracked for a longer period of time. The lowest threshold was 40 dBZ, used for the weak 5 June 2012 case (Table 1). If the second-tier reflectivity region exceeded another specified area threshold, the entire 35 dBZ composite reflectivity area was then counted as a convective cell. Both the 35 dBZ and second-tier area thresholds were varied between cases so that each case was optimally tracked in a subjective sense.

2.5. Calculation of Storm Parameters

Storm parameters were calculated by indexing the gridded vertical velocity, HID, and reflectivity data over the cell areas (35 dBZ regions) identified by the CLEAR software. To select appropriate bounds over which to calculate storm parameters, a volume enclosing each cell was defined. This volume is represented by the cell area (35 dBZ composite reflectivity region) in the horizontal and extends through all vertical levels of the radar grid. Using temperature levels interpolated from environmental proximity soundings, the enclosing cell volume was then constrained to vertical levels within the mixed-phase region. Hydrometeor echo volumes were calculated by summing the number of grid boxes within the mixed-phase storm volume for which the HID identified a given hydrometeor as the dominant particle type. This number was multiplied by the volume of a single grid box to arrive at the total volume. Using combined HID output and reflectivity data, the precipitating ice mass was calculated. For each grid box identified as containing graupel or hail, the reflectivity

Table 1. Summary of Storm Type, Severe Characteristics, and Total Lightning Activity for Each Colorado Storm Studied[a]

Case Name	Analysis Period (HH:MM UTC)	Storm Type; Severe Reports	Mean TFR (min^{-1})	Max TFR (min^{-1})	Dual-Doppler Synthesis
5 June 2012	22:25–23:35	single cell; nonsevere	1.1	5.2	yes
6 June 2012 storm 1	21:05–21:55	single cell; nonsevere	25.6	94.6	yes
6 June 2012 storm 2	21:30–23:30	supercell; 3.8 cm hail	107.3	169.7	no
6 June 2012 storm 3	23:00–00:18 7 June	single cell; 2.5 cm hail	48.0	92.3	yes
6 June 2012 storm 4	23:06–00:18 7 June	single cell; nonsevere	40.3	87.5	yes
22 June 2012 storm 1	22:35–23:45	supercell; severe warned	115.6	223.0	no
22 June 2012 storm 2	23:50–00:50 23 June	single cell; nonsevere	35.3	140.4	no
27 June 2012	21:55–22:50	single cell; nonsevere	13.8	54.4	yes
28 June 2012	20:40–22:00	single cell; nonsevere	8.1	26.4	yes
17 June 2013 (CHILL-MIE)	20:55–23:00	supercell; severe warned	29.8	58.4	yes
3 August [b](CHILL-MIE)	21:14–23:36	supercell; 4.4 cm hail, tornado	168.5	287.8	no

[a]The first and second columns list the date and analysis period for each storm. The third column lists the subjectively identified storm type (single cell thunderstorm, multicell, or supercell) and any associated severe warnings or severe storm reports. Severe storm reports were obtained from the NWS Storm Prediction Center. The fourth and fifth columns list the mean and maximum total flash rates (Mean TFR and Max TFR) determined by the DBSCAN-based flash-counting algorithm. The yes/no statements in the final column indicate whether dual-Doppler wind retrievals were performed.
[b]Polarimetric WSR-88DP radar data were used, not CHILL data.

was converted to mass using separate reflectivity-mass (*Z-M*) relationships for graupel and hail derived by *Heymsfield and Miller* [1988]. The masses in all identified grid boxes were then summed.

Reflectivity echo volumes were calculated by summing the number of grid boxes with reflectivity above some threshold (e.g., 35 dB*Z*) and multiplying by the grid box volume. Updraft volumes above a given vertical velocity threshold were calculated the same way. The maximum vertical velocity was calculated by simply finding the absolute maximum in updraft for all grid points in the mixed-phase region. The cloud-top height was calculated as the maximum height of the 20 dB*Z* radar echo, following *Barthe et al.* [2010]. The product of precipitating and nonprecipitating ice mass flux (P_{flux}) was calculated following the divergence method described by *Deierling et al.* [2008], although in contrast to that study, the flux product calculation was constrained to the enclosing cell volume described at the beginning of this section. Nonprecipitating ice masses were calculated using a *Z-M* relationship developed by *Heymsfield and Palmer* [1986].

2.6. Flash Counting

For this study, it was necessary to identify individual lightning flashes from the LMA data and attribute the identified flashes to individual storms. As discussed in section 1, LMA networks offer one of the few means to observe total lightning activity in storms [*Rison et al.*, 1999]. A minimum of four different LMA stations is required to pinpoint the time and location of a VHF source emitted by electrical breakdown [*Thomas et al.*, 2004]; the northern Colorado LMA (COLMA) network consists of 15 stations to reduce errors in estimates of VHF source locations and times (although at any given time, there were often only 7–10 stations in operation). The network has excellent sensitivity as the area containing the LMA has few VHF noise sources [*Rison et al.*, 2012]. It was assumed that the COLMA reliably detected 100% of lightning flashes within 200 km of the network center, a range over which climatological flash rates derived from COLMA data have been found to be relatively constant (B. R. Fuchs et al., Utilities of an open-source LMA flash-clustering algorithm, *J. Geophys. Res.*, in preparation). The 200 km detection range encloses all 11 Colorado storms sampled.

This study uses automated flash-counting software to sort VHF sources into lightning flashes. The software, developed by E. Bruning at Texas Tech University and B. Fuchs at CSU [*Fuchs et al.*, 2015a], uses a Density-Based Spatial Clustering of Applications with Noise (DBSCAN) algorithm [*Ester et al.*, 1996] implemented in the Python programming language [*Bruning*, 2013]. This flash-counting software will be referred to as the DBSCAN-based software. *Fuchs et al.* [2015a] first used the DBSCAN-based software and found that flash counts were usually within 10–15% of flash counts using the detailed XLMA software, considered the standard tool for LMA data analysis [*Thomas et al.*, 2003].

The DBSCAN-based software works differently from other LMA flash algorithms such as XLMA. First, the software identifies lightning flashes by finding high-density clusters of VHF sources (density-connected sources,

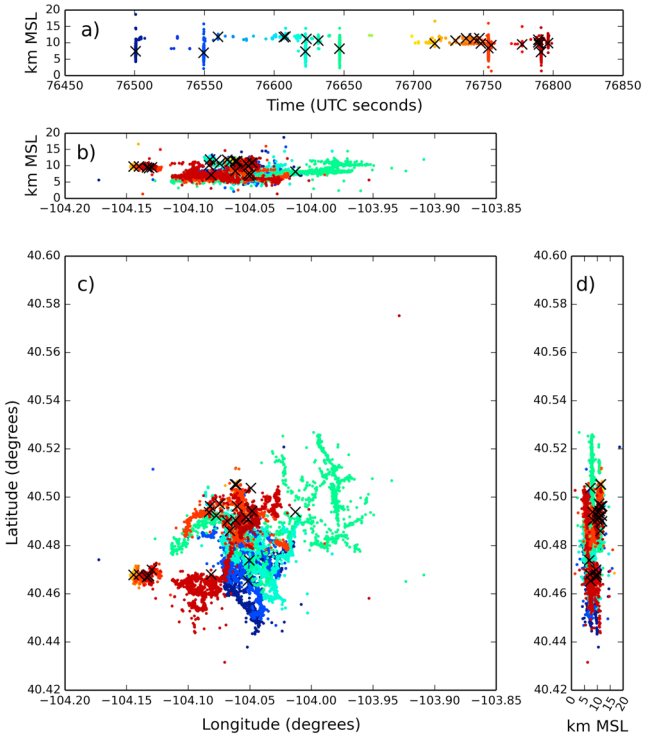

Figure 2. Multipanel plot showing VHF sources (colored points) detected by the Colorado LMA for the 5 min period beginning at 21:14:59 UTC on 6 June 2012. Sources are colored by time from blue to red. Each cross marks a cluster of sources identified by the algorithm as a single lightning flash. (a) All sources and identified flashes in a time-height projection, with height in kilometers and time in seconds (UTC); (b) all sources and flashes in a longitude-height vertical cross section; (c) all sources and flashes in a latitude-longitude (plan) projection, and (d) all sources and flashes in a latitude-height vertical cross section.

as defined by *Ester et al.* [1996]) residing within 3 km in space and 150 ms in time from an initial VHF source point. These spatial and temporal thresholds were advocated by *MacGorman et al.* [2008] to satisfactorily sort VHF sources into flashes. However, while other algorithms simply associate all VHF points within these thresholds with a flash, the application of the high-density criterion is unique to the DBSCAN-based software. Then, for an identified VHF high-density source cluster to be counted as a lightning flash, it was required that a minimum of 10 sources be associated with that cluster. Once a cluster (flash) is defined, DBSCAN continues to search for additional sources to be associated with that flash. All additional sources again must reside no more than 3 km in space and 150 ms in time from any source already associated with the flash. Finally, for all DC3 cases, a VHF source must have been detected by at least seven of the stations in the COLMA network to be counted as part of a flash. For the two 2013 CHILL-MIE cases (Table 1), a six-station threshold was used because only six stations were regularly operational during the times that these two cases occurred. Although the six-station threshold is less ideal in terms of reducing VHF noise, it was deemed necessary in order to have sufficient VHF source data to calculate physical flash rates.

In addition to the technical differences just described, the DBSCAN-based algorithm is implemented in an automated manner, offering practical advantages over XLMA when processing large LMA data sets. The DBSCAN-based software was merged with the CLEAR cell-tracking output (section 2.4) to objectively associate a lightning flash with the storm that produced it, as discussed later in this section. In contrast, XLMA is run through a graphical user interface, requiring the user to subjectively define the time and space domains over which lightning flashes are counted based on visual maps of LMA-detected VHF sources. XLMA is cumbersome to use when vigorous convective cells occur in close proximity, in which case it is difficult to visually distinguish VHF sources from separate cells. The increased objectivity and efficiency afforded by the DBSCAN-based software motivated its use in the present study.

Figure 2 shows VHF sources and flashes detected by the COLMA and flashes identified by the algorithm during one 5 minute period. In a qualitative sense, the DBSCAN-based software appears to correctly identify lightning flashes. In addition to total flash counts, the software calculates the convex hull area of each flash, described by *Bruning and MacGorman* [2013] as the minimum area enclosing a horizontal projection of all VHF sources associated with a given flash. A representative size, or flash extent, for each individual flash was also determined by taking the square root of the convex hull area, following *Bruning and MacGorman* [2013]. A flash extent has linear units and was taken to be representative of the flash channel length.

Identified lightning flashes were merged with CLEAR cell-tracking output to objectively attribute lightning flashes to tracked cells. Lightning flashes were attributed to storms if their initiation location occurred within identified 35 dBZ regions (cells). To account for lightning flashes that occurred outside of the main

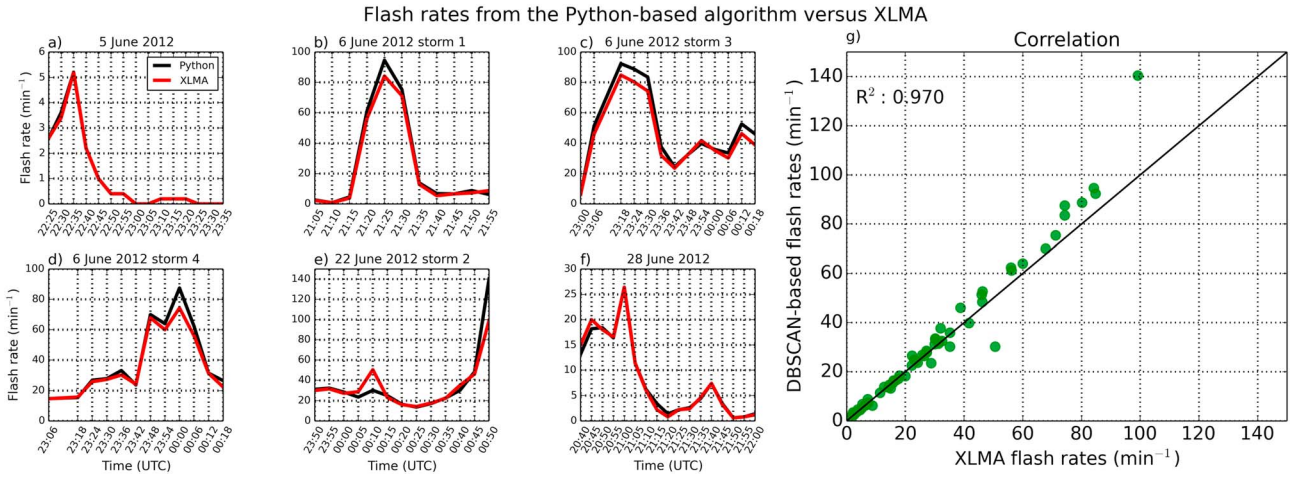

Figure 3. Flash rate time series calculated using the DBSCAN-based algorithm (black) and using the XLMA software (red) for the (a) 5 June 2012, (b) 6 June 2012 storm 1, (c) 6 June 2012 storm 3, (d) 6 June 2012 storm 4, (e) 22 June 2012 storm 2, and (f) 28 June 2012 cases; (g) scatterplot of all flash rates calculated using the DBSCAN-based algorithm (*y* axis) versus using the XLMA software (*x* axis) for these six storms. The coefficient of determination (R^2) is indicated on the plot, and a black line representing the equation $y = x$ to indicate one-to-one correspondence is also shown.

convective cores (e.g., in storm anvils), flashes within 10 km of an identified cell were also attributed. If an identified flash was within 10 km of more than one cell, it was attributed to the nearest cell. Table 1 provides a brief summary of lightning activity, storm mode, and severe characteristics for all Colorado storms sampled. Mean and maximum flash rates are reported as well as the time period over which each storm was tracked and whether a dual-Doppler analysis was performed. Each storm is referred to by the date on which it was first identified and tracked by CLEAR. Multiple cases that occurred on a single day are further labeled in chronological order based on when the analysis period began.

To assess the accuracy of the DBSCAN-based flash-counting algorithm, flash rates calculated using this algorithm were compared to flash rates calculated using the standard XLMA software [*Thomas et al.*, 2003] for six of the 11 cases analyzed: the 5 June storm; 6 June storms 1, 3, and 4; 22 June storm 2; and the 28 June 2012 case (Table 1). These storms were selected from the larger 11-storm sample because they were relatively isolated and therefore straightforward to flash count with XLMA. Figure 3 shows that the flash rates from the DBSCAN-based software are in close agreement with those diagnosed by the XLMA software for each of these six storms (Figures 3a–3f). The largest differences occurred for flash rates exceeding 30 min^{-1}, with calculated flash rates typically exceeding those determined by XLMA. For these high flash rates, which included 26 of the 81 flash rate observations comprising this six-storm sample, the DBSCAN-based flash rates differed from XLMA by 11.3% on average. When flash rates are large, the DBSCAN-based software may tend to break up some flashes into multiple smaller flashes, a common problem of many flash-counting algorithms [*Bruning*, 2013]. The deviation of the high flash rates from a one-to-one correspondence to XLMA is shown in Figure 3g. However, that the differences are relatively small (within 12%) is evidence of the accuracy of the DBSCAN-based algorithm. Additionally, although XLMA is considered the standard LMA analysis tool, it is difficult to determine the accuracy of XLMA. In this sense, the observed differences from XLMA should not be interpreted with certainty as inaccuracies in flash counts.

2.7. Large National Mosaic and Multisensor Quantitative Precipitation Estimation Radar Reflectivity Data Set

To rigorously test modified flash rate parameterizations and assess their performance in different thermodynamic and kinematic environments (section 4), an expansive data set containing gridded radar reflectivity data for thousands of thunderstorm cells in four different regions was prepared. The cells occurred in the regions of northeastern Colorado (CO, 726 cells), central Oklahoma (OK, 703), northern Alabama (AL, 1351) and in the vicinity of Washington, D.C. (DC, 1542), for a total of 4322 cell observations. These cells were identified and analyzed by *Fuchs et al.* [2015a] using the National Mosaic and Multisensor Quantitative Precipitation Estimation (NMQ) radar reflectivity product [*Zhang et al.*, 2011]; a more complete discussion of the analysis can be found therein. The four regions were selected because each is centered on an LMA network, allowing for total lightning flash rates for each cell to be determined. It was required that all 4322 selected cells be

isolated and within 125 km of their respective LMA network center so that flash rates could be reliably calculated. The same CLEAR framework (section 2.4) was used by *Fuchs et al.* [2015a] to identify and track the cells, and the DBSCAN-based flash-counting algorithm discussed in section 2.6 was used to determine total flash rates. Different thresholds were used for the Alabama and Washington, D.C., LMA data sets for associating VHF sources with flashes to account for the lower sensitivities of these networks: an identified VHF source cluster was required to contain a minimum of two VHF sources to be counted as a flash, the sources could be separated by no more than 6 km in space, and a minimum of six stations were required to have detected a given VHF source for it to be associated with a flash.

The NMQ radar reflectivity product is on a 0.01° × 0.01° latitude-longitude horizontal grid, and the stretched vertical grid spacing varied from 0.25 km at the bottom of the domain to 2.0 km at the top for the NMQ data used by this study [*Zhang et al.*, 2011]. Each tracked cell may be considered to be equivalent to a single storm volume as discussed at the beginning of this section. *Fuchs et al.* [2015a] also attributed time-interpolated local environmental data from Rapid Refresh model analyses to each cell to characterize a cell's thermodynamic buoyancy profile and warm cloud depth, among other environmental parameters. Model-derived environmental data were attributed to cells by adapting the method of *Potvin et al.* [2010] to find the model sounding best representative of cell inflow air. In the present study, the mean wind direction in the lowest 75 hPa at a cell's forecasted position was calculated, and data at the model grid point along this direction and immediately adjacent to the cell's forecasted position were attributed. This method is thought to objectively represent inflow air that will be imminently ingested by a cell. NCAPE for every cell was calculated from the attributed model environmental profile by dividing CAPE by the CAPE depth (H_{CAPE}) as defined in section 1. To avoid unrealistically large values of NCAPE that resulted when CAPE was confined over a shallow depth, NCAPE was set to zero for $H_{CAPE} < 2.5$ km. The H_{CAPE} threshold needed to be applied to only 4.6% of the total population of cells; i.e., unphysical NCAPE values were rare. Different H_{CAPE} thresholds up to 5 km were also tested, but for all samples with $2.5 < H_{CAPE} < 5$ km, NCAPE values were physical (NCAPE < 0.1 m s^{-2}), so the 2.5 km H_{CAPE} threshold was chosen.

3. Results

3.1. Evaluation of Existing Flash Rate Parameterizations

The five parameterizations from the literature (section 1) that were tested against the 11 Colorado DC3/CHILL-MIE cases are summarized in Table 2. The equations describing the relationships between each storm parameter and flash rate are listed, along with the root mean square error (RMSE) and normalized root mean square error (NRMSE) for each scheme when tested against the Colorado data set. NRMSE is defined herein as RMSE divided by the range of all observed flash rates. These error statistics were calculated over all 183 data points for the PR92CTH and D08P schemes, and over the 96 samples for which the vertical wind field was retrieved for the other three schemes. It is readily apparent that the five flash rate parameterizations tested do not consistently predict total flash rates well for this sample of storms. RMSE values are large, exceeding 75 flashes per minute for the PR92CTH and D08P schemes. The scheme with the lowest NRMSE is PR92W, but even this scheme was in error by nearly 23% on average. The normalized mean bias error (NMBE), calculated as the mean bias divided by the range of observed flash rates, is large and negative for all schemes (Table 2), reflecting the existing schemes' frequent prediction of negative flash rates and inability to predict the high flash rates observed in the sampled Colorado storms (Figure 4).

Flash rate time series predicted by each parameterization are shown in Figure 4 along with observed flash rates (black curves) determined by the DBSCAN-based flash-counting algorithm for the 11 Colorado thunderstorms (observed flash rate time series will be consistently denoted by black curves). These plots show that the errors of the existing schemes are even worse than suggested by the bulk error statistics in Table 2. Some schemes significantly underestimated flash rates (e.g., the PR92CTH and D08P schemes), while others (notably the D08F scheme) did not predict any flash rate variability at all. The poor performance of the D08P and D08F schemes may in part be due to the different HID used in this study versus *Deierling et al.* [2008] to calculate the requisite storm parameters. The DP08 and D08P schemes also often predicted unphysical negative flash rates due to their negative constant coefficients (Table 2). The PR92W scheme (green curve) predicted flash rates well for the 5 June 2012 case (Figure 4a), and while the PR92CTH overestimated flash rates, it predicted the overall flash rate trend. However, the PR92CTH scheme performed poorly for the other 10 storms, whose flash rates were generally much larger than those produced by the 5 June 2012 case (Table 1). In general, the existing schemes are not sufficiently sensitive to predict the large range and variability of flash rates observed in the

Table 2. Summary of Existing Flash Rate Parameterization Schemes From the Literature That Were Tested Against Observations of the Storms Summarized in Table 1[a]

Parameter (Units)	Equation	Reference	Sample Size	RMSE (min^{-1})	NRMSE (%)	NMBE (%)
Maximum vertical velocity ($m\ s^{-1}$)	$f = (5.0 \times 10^{-6}) \times W_{max}^{4.5}$	*Price and Rind* [1992] (PR92W)	96	21.6	22.8	−9.9
Cloud-top height (km)	$f = (3.44 \times 10^{-5}) \times H^{4.9}$	*Price and Rind* [1992] (PR92CTH)	183	79.0	27.4	−18.0
Updraft volume >5 $m\ s^{-1}$ (km^3)	$f = (6.75 \times 10^{-2}) \times UV5 - 13.9$	*Deierling and Petersen* [2008] (DP08)	96	30.8	32.5	−25.8
Precipitating ice mass (kg)	$f = (3.4 \times 10^{-8}) \times PIM - 18.1$	*Deierling et al.* [2008] (D08P)	183	85.9	29.9	−23.2
Ice mass flux product ($kg^2\ m\ s^{-2}$)	$f = (9.0 \times 10^{-15}) \times P_{flux} + 13.4$	*Deierling et al.* [2008] (D08F)	96	26.6	28.1	−10.9

[a]The first column lists the storm parameter used to predict flash rate, the second column lists the derived mathematical relationship between each parameter and flash rate (f), and the third column lists the reference for each flash rate-storm parameter relationship. The final four columns list the sample size against which each parameterization scheme was tested, the root mean square error, the normalized root mean square error, and the normalized mean bias error calculated over all samples.

Colorado storms studied. Although only 11 storms were sampled, the consistently poor performance of the existing schemes warrants modification of the parameterization coefficients to improve prediction of flash rate in these, and likely other, Colorado storms.

3.2. Modification of Existing Flash Rate Parameterizations

Coefficients of the existing flash rate parameterizations were modified by quantifying the relationship between flash rate and storm parameters observed for the 11 sampled storms. A modified parameterization based on PIM and parameterizations based on similar quantities including the graupel echo volume (GEV) and

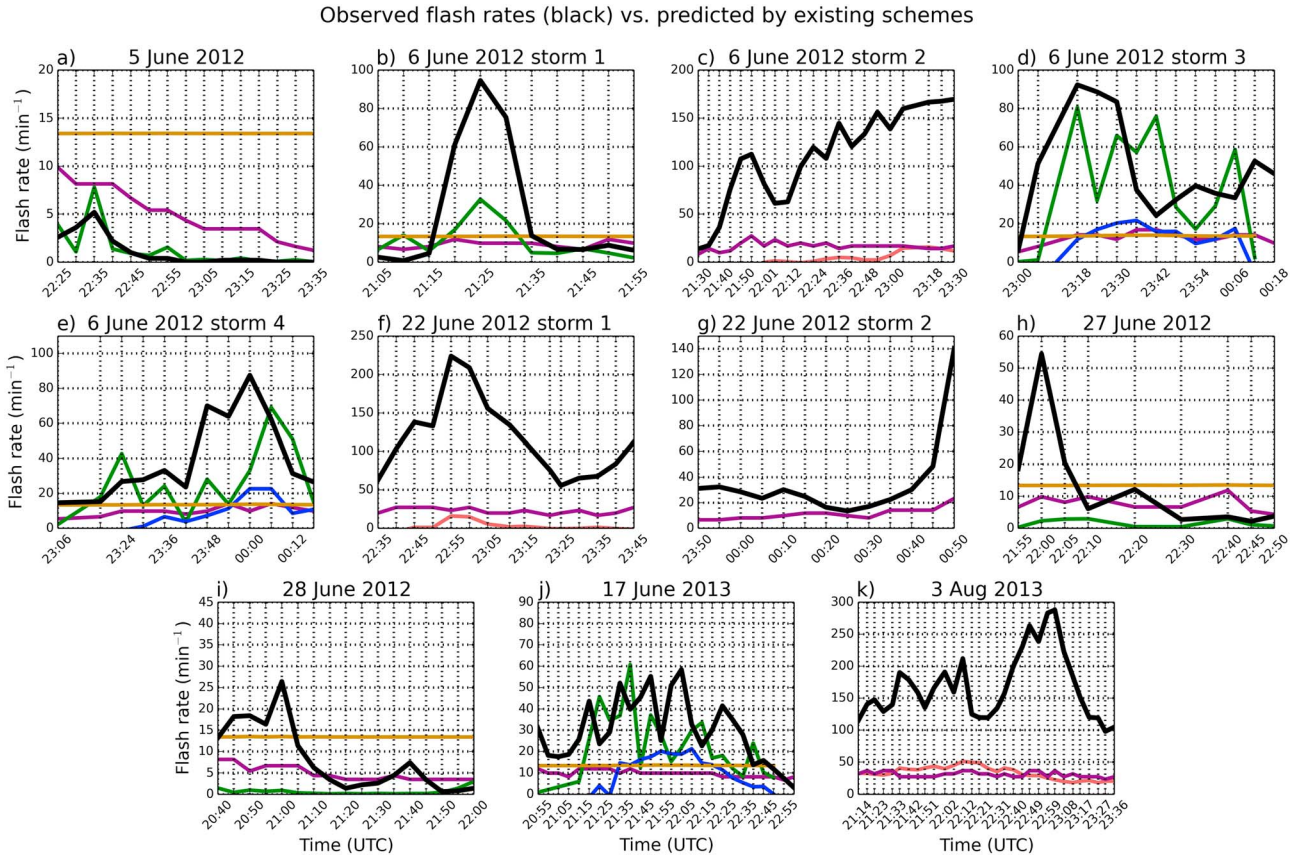

Figure 4. Eleven-panel plot showing observed flash rates (black curves) versus flash rates predicted by the PR92W (green), PR92CTH (purple), DP08 (blue), D08P (pink), and D08F (gold) schemes for all sampled Colorado thunderstorms described in Table 1. Flash rates predicted by the PR92W, DP08, and D08F schemes are not shown in Figures 4c, 4f, 4g, and 4k because the vertical wind field was not retrieved for these cases. Flash rates predicted by DP08 are not shown in Figures 4a, 4b, 4h, and 4i because they did not lie within the range of plotted data (unphysical negative flash rates were predicted). Flash rates predicted by D08P are not shown in Figures 4a, 4b, 4d, 4e, and 4g–4j for the same reason.

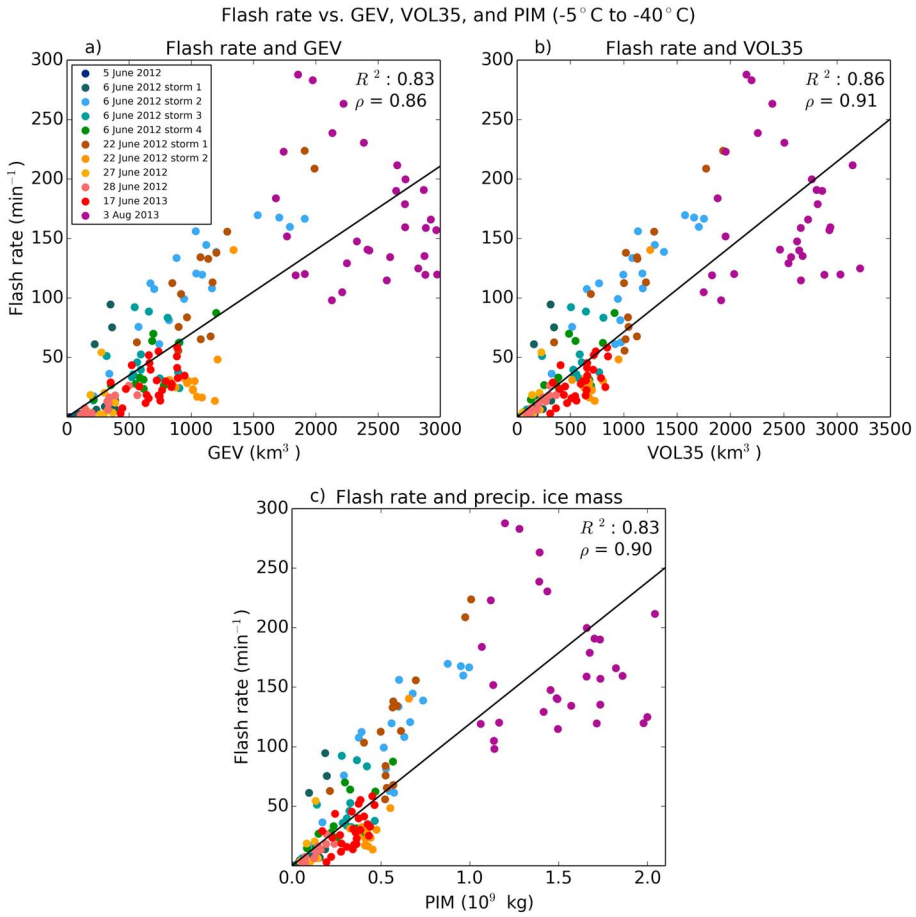

Figure 5. Scatterplots of total lightning flash rate versus (a) GEV, (b) VOL35, and (c) PIM in the mixed-phase region for all Colorado storm volumes. Each point corresponds to a different storm volume; the colors denote all storm volumes from one particular case. The coefficient of determination (R^2) of each least squares fit and Spearman's rank correlation coefficient (ρ, which ranges from zero to one to assess the degree to which the relationship is monotonic) are indicated on each subplot; best fit trend lines are indicated in black.

the mixed-phase 35 dB*Z* echo volume (VOL35) were developed. To develop these parametric relationships, LMA-derived flash rates for each of the 183 storm volumes were regressed against corresponding observations of GEV, VOL35, and PIM using a least squares technique. Scatterplots depicting the relationship between each storm parameter and flash rate and the resulting linear regression are shown in Figure 5. A simple linear trend with an intercept passing through the origin was found to fit each data set well. An intercept of zero also avoided solutions potentially containing a negative constant coefficient, a problem encountered when applying some of the existing flash rate schemes. All three storm parameters were robustly correlated to flash rate, indicated by a coefficient of determination (R^2) of 0.83, 0.86, and 0.83 for GEV, VOL35, and PIM, respectively. The solution to each least squares fit is given in Table 3 along with the RMSE and NRMSE for each scheme, calculated over all 183 Colorado storm volumes. The average errors of the GEV, VOL35, and PIM schemes are reduced by more than a factor of 2 in comparison to the PR92CTH and D08P schemes.

The qualitative performance of these schemes for the 11 Colorado cases is shown in Figure 6. Predicted flash rates are shown alongside observed flash rate time series for each case to assess whether flash rate magnitudes were generally predicted well and whether these modified schemes predicted more flash rate variability than the existing schemes (Figure 4). The GEV, VOL35, and PIM schemes correctly predicted the general flash rate trend for most cases and represent a significant improvement over existing parameterizations. Predicted flash rate time series match observed time series especially well for the 6 June 2012 storm 4, 28 June 2012, and 17 June 2013 cases (Figures 6e, 6i, and 6j). In contrast to the existing schemes discussed in section 3.1, the modified schemes successfully predicted the high flash rates observed in these storms. For a few storms, peak flash rates were incorrectly predicted by a significant margin. For the 6 June 2012 storm 1 case (Figure 6b),

Table 3. Summary of Updated Flash Rate Parameterization Schemes[a]

Parameter (Units)	Equation	Sample Size	R^2	RMSE (min^{-1})	NRMSE (%)
Graupel echo volume (km^3)	$f = (7.0 \times 10^{-2}) \times GEV$	183	0.83	39.0	13.6
35 dBZ echo volume (km^3)	$f = (7.2 \times 10^{-2}) \times VOL35$	183	0.86	35.6	12.4
Precipitating ice mass (kg)	$f = (1.2 \times 10^{-7}) \times PIM$	183	0.83	38.6	13.4
Updraft volume > 5 m s^{-1} (km^3)	$f = (1.1 \times 10^{-1}) \times UV5$	96	0.72	18.1	19.1
Updraft volume > 10 m s^{-1} (km^3)	$f = (2.1 \times 10^{-1}) \times UV10 + 8.8$	96	0.49	17.4	18.4
Maximum vertical velocity (m s^{-1})	$f = 1.9 \times W_{max} - 16.7$	96	0.47	17.8	18.8
Ice mass flux product (kg^2 m s^{-2})	$f = (4.1 \times 10^{-8}) \times P_{flux}^{0.64}$	96	0.52	19.0	20.0

[a]The first column lists the storm parameter used to predict flash rate, and the second column lists the derived mathematical relationship between each parameter and flash rate (f). The final four columns list the sample size of storm volumes from which each scheme was developed, the coefficient of determination of the fit (R^2), the root mean square error (RMSE), and the normalized root mean square error (NRMSE) calculated over all samples.

peak flash rate is underestimated by all three schemes by almost a factor of 5, and the early flash rate peak at 22:00 UTC for the 27 June 2012 case is underestimated by more than a factor of 2 (Figure 6h). However, even when peak flash rates were underestimated (e.g., 6 June 2012 storm 2, Figure 6c), the general flash rate trend was captured, in contrast to the existing schemes (Figure 4c). All three schemes also predicted flash rates similar to one another, suggesting that the simplest VOL35 scheme, which requires radar reflectivity information only, may be the most useful of the three schemes.

To quantify the performance of the GEV, VOL35, and PIM schemes, error statistics for each scheme were calculated for the 11 Colorado storms individually and are shown in Figure 7. Figure 7a shows RMSE for each case, and Figure 7b shows the corresponding NRMSE, now calculated by dividing the RMSE by the range of

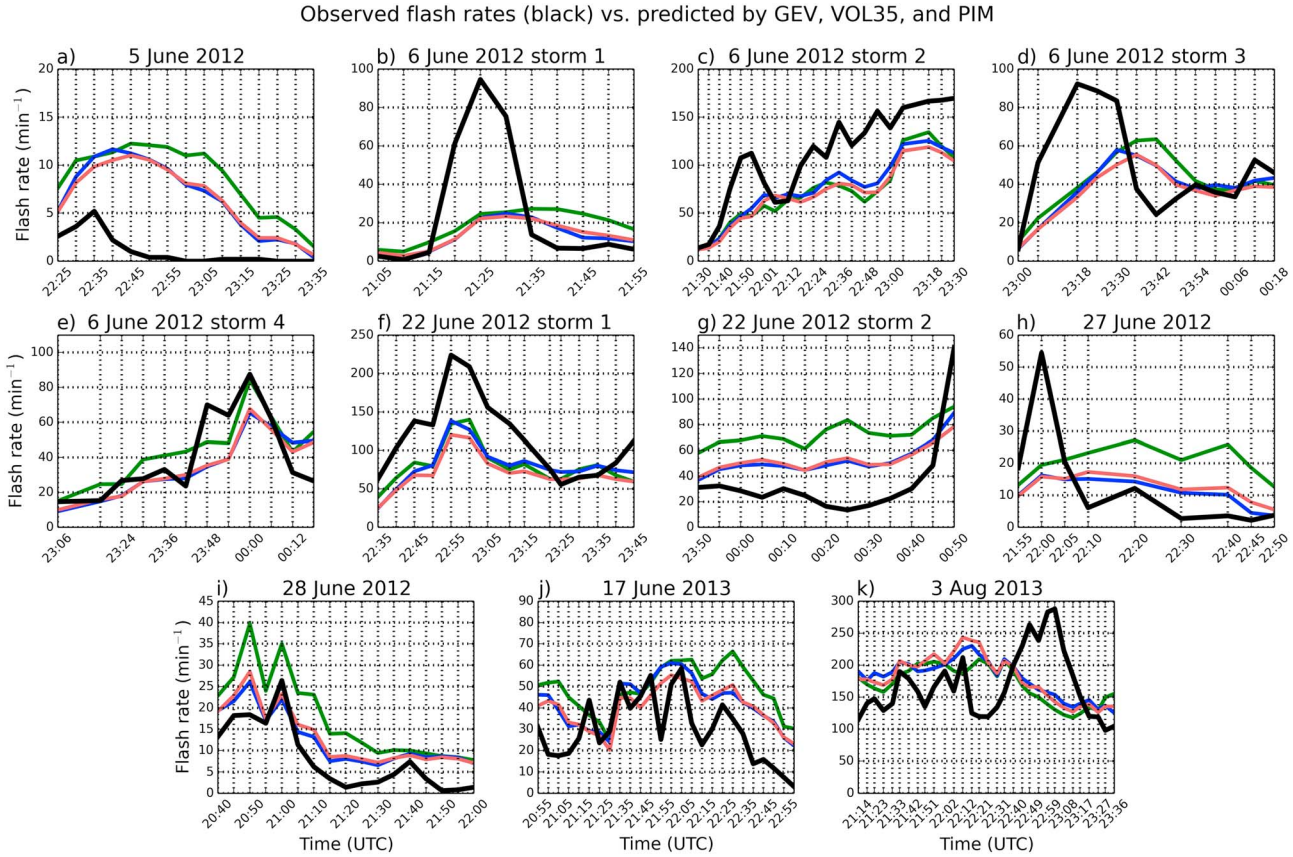

Figure 6. Eleven-panel plot showing observed flash rates (black curves) versus flash rates predicted by the GEV (green), VOL35 (blue), and PIM (pink) schemes for all sampled Colorado thunderstorms described in Table 1.

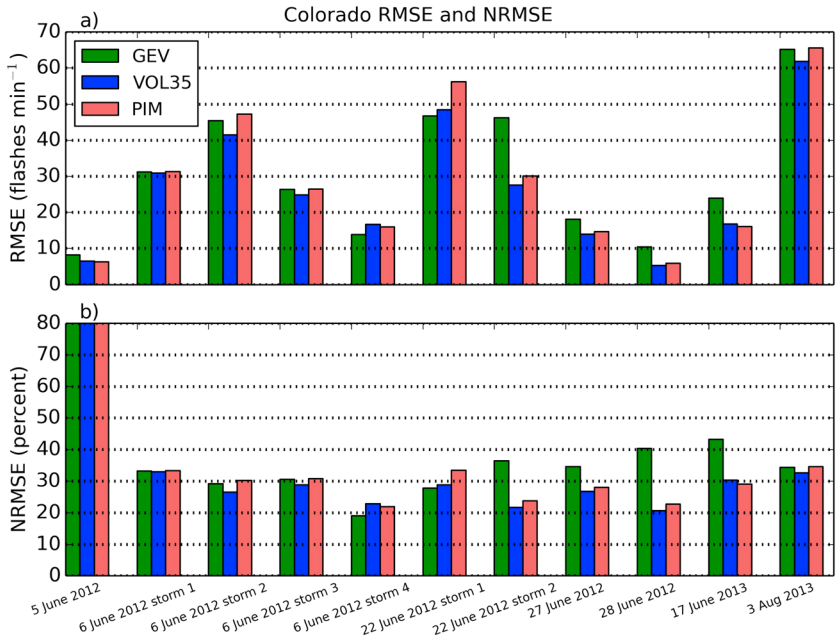

Figure 7. Bar plots of (a) root mean square error (RMSE) and (b) normalized root mean square error (NRMSE) for the updated GEV, VOL35, and PIM schemes for each Colorado case. Green bars represent errors for the GEV scheme, blue for the VOL35 scheme, and pink for the PIM scheme.

observed flash rates for each individual storm. The VOL35 scheme exhibited some of the lowest errors for individual cases (Figure 7) and the lowest NRMSE overall (12.4%, Table 3). The GEV scheme performed similarly to the VOL35 scheme but had larger errors for some cases (e.g., the 22 June 2012 storm 2, 28 June 2012, and 17 June 2013 cases). The NRMSE for the 5 June 2012 case was large because the range of observed flash rates was only 5 min^{-1}; note that the RMSE for this case is less than 10 min^{-1}. For other cases, the VOL35 NRMSE was below 25% (e.g., 6 June 2012 storm 4, 22 June 2012 storm 2, and 28 June 2012). The PIM scheme performs nearly equally as well as the VOL35 scheme, suggesting that explicit knowledge of precipitating ice mass may not be necessary, avoiding the application of uncertain *Z-M* relationships. The success of the simpler VOL35 scheme is encouraging because it suggests that this scheme may be useful when applied to a larger sample size or in real time when only storm reflectivity data are available. This topic will be investigated in the next section.

Recall that despite the success of the GEV, VOL35, and PIM schemes, large, brief fluctuations in flash rate were sometimes poorly predicted, such as the early flash rate peak observed for the 27 June 2012 case (Figure 6h). Updraft parameters were therefore also investigated as predictors of flash rate to possibly improve the PR92W, DP08, and D08F schemes and to investigate whether variations in these updraft parameters were associated with additional flash rate variability. Past studies have noted that rapid increases in updraft intensity and volume often accompanied sharp, sudden increases in flash rate [e.g., *Wiens et al.*, 2005]. Updraft parameters investigated included the mixed-phase updraft volume greater than 5 and 10 m s^{-1} (UV5 and UV10, respectively), the maximum observed updraft in the mixed-phase region (W_{max}), and the product of precipitating and nonprecipitating ice mass flux (P_{flux}), all of which have been shown by past studies to be well correlated to lightning activity.

The results of the regressions between flash rate and UV5, UV10, W_{max}, and P_{flux} are shown in Figure 8 and are also summarized in Table 3 (a power law parameterization was developed for P_{flux} because its relationship to flash rate was observed to be somewhat nonlinear). None of the updraft parameters are as well correlated to flash rate as the GEV, VOL35, and PIM storm parameters. Note that several data points are offset significantly above the best fit trend lines (most evident in Figures 8a and 8b), adversely affecting the correlation. This offset is unlikely to be explained by flash-counting errors, given the close agreement between calculated flash rates and flash rates determined using the XLMA software (section 2.6). *Carey et al.* [2014, Figure 5] developed a series of lightning parameterizations based on observations of Alabama storms during DC3 and likewise observed what they referred to as a bifurcation in the relationship of flash rate to updraft variables. In their study, graupel echo volume, a similar quantity to VOL35, was found to be the superior predictor of flash rate.

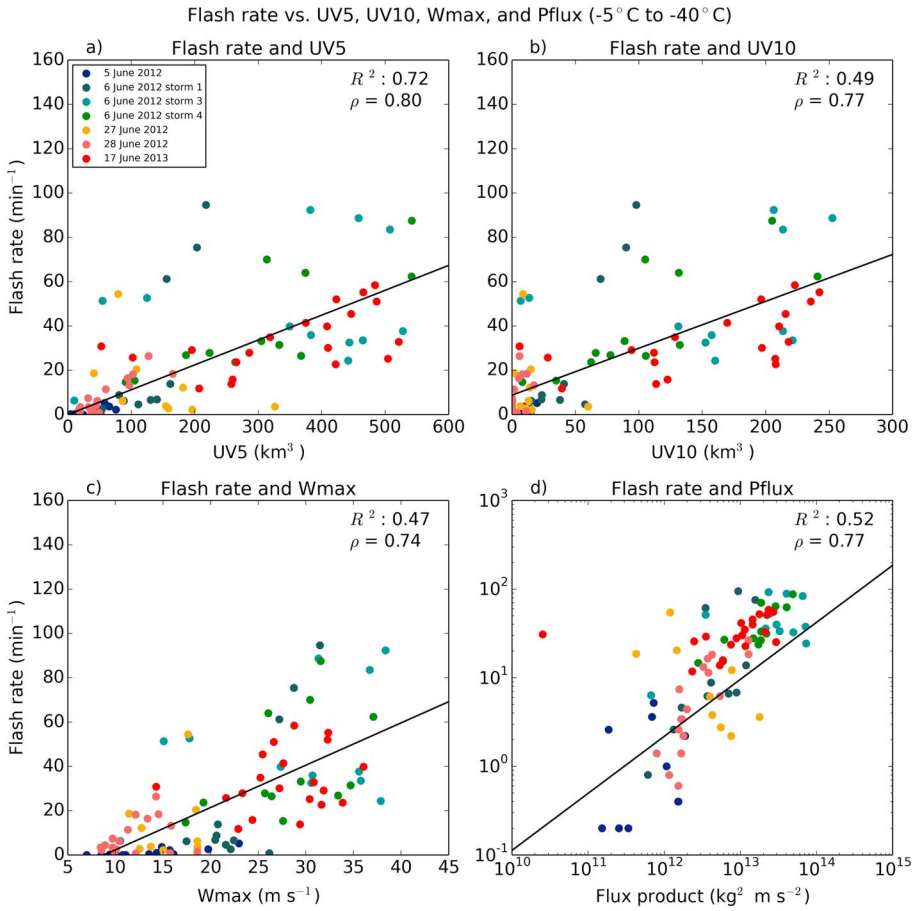

Figure 8. Scatterplots of total lightning flash rate versus (a) UV5, (b) UV10, (c) W_{max}, and (d) P_{flux} for all Colorado storm volumes. Each point corresponds to a different storm volume; the colors denote all storm volumes from one particular case. The coefficient of determination (R^2) of each least squares fit and Spearman's rank correlation coefficient (ρ) are indicated on each subplot; best fit trend lines are indicated in black.

These results contrast with previous studies that found strong relationships between flash rate and updraft characteristics such as *Deierling and Petersen* [2008, Figure 2], although that study did observe a large scatter in UV5 for flash rates less than 100 min^{-1}, similar to what is observed herein. Importantly, updraft variables did not explain additional flash rate variability that the GEV, VOL35, and PIM schemes did not already explain, so predicting flash rate based on combinations of updraft and ice mass variables (e.g., the product of UV10 and GEV) did not yield significant improvement. Due to the comparatively weak relationships shown in Figure 8, as well as the performance of the PR92W, DP08, and D08F schemes discussed in section 3.1, updraft parameters are not recommended to predict flash rates for this sample of Colorado storms. Although modeling studies frequently employ lightning parameterizations based on updraft parameters such as W_{max} [e.g., *Pickering et al.*, 1998; *Fehr et al.*, 2004], the performance of several modified parameterizations suggests that VOL35 is a superior proxy for flash rate, particularly for Colorado storms.

4. Broader Applicability of Flash Rate Parameterizations

It has been shown that lightning flash rates are well predicted for the sampled Colorado storms by bulk storm volume quantities like VOL35. It was also suggested that the VOL35 scheme could be used to predict flash rates for a much larger sample of storms. The VOL35 scheme was therefore tested on the large data set of thunderstorm cells spanning multiple regions described in section 2.7 in order to answer the second question posed by this study: are flash rate parameterizations applicable in multiple regions characterized by different environmental conditions? Testing of updated schemes (Table 3) was necessarily limited to the VOL35 scheme since the NMQ product contains radar reflectivity information only. The existing PR92CTH scheme, which also

Table 4. Definitions of the NCAPE, WCD, and Surface-6 km Shear Bins Discussed in the Text and Shown in Figure 9[a]

Parameter (Units)	Low (Shallow)	Moderate	High (Deep)	Extreme
NCAPE (m s^{-2})	<0.1	0.1–0.2	0.2–0.3	>0.3
WCD (km)	<1.0	1.0–2.0	2.0–3.0	>3.0
Shear (knots)	<20.0	20.0–40.0	40.0–60.0	>60.0

[a]The low and high categories apply to NCAPE and shear, whereas the shallow and deep categories apply to WCD.

requires reflectivity information only, was tested as well to compare its performance on a large sample of storms to the VOL35 scheme.

All 4322 cells from the NMQ data set were separated into their respective regions (CO, OK, AL, and DC) and also binned into NCAPE, WCD, and surface-6 km vertical wind shear categories defined in Table 4 to evaluate the performance of the VOL35 scheme as a function of environment. Simple error statistics were examined as a function of each region and each environmental parameter. Figure 9 shows the NRMSE as a function of region and the various NCAPE, WCD, and shear categories (Table 4). Since each cell is treated as a unique storm volume in the CLEAR framework, these NRMSE statistics may be compared to those presented in Table 3, which were calculated over the 183 Colorado storm volumes. When tested on this substantially larger set of independent storm volumes, the VOL35 scheme performs excellently. The NRMSE is 5.8% for all 4322 cells (Figure 9a), lower than the NRMSE of the VOL35 scheme for the Colorado cases used to develop the parameterization (12.4%, Table 3). When error statistics are calculated by region, the scheme is most successful in Colorado, with NRMSE of 7.2%, but also performs comparably well in all regions, with NRMSE always below 10%. As a function of environmental parameters, the VOL35 scheme is most successful in low NCAPE, moderate WCD, and moderate vertical wind shear environments, and its error generally increases with increasing values of each environmental parameter.

The largest average errors occurred for the extreme NCAPE environment defined in Table 4 (35.5%, Figure 9b), in which thunderstorm cells were large but did not always produce proportionally higher flash rates. More

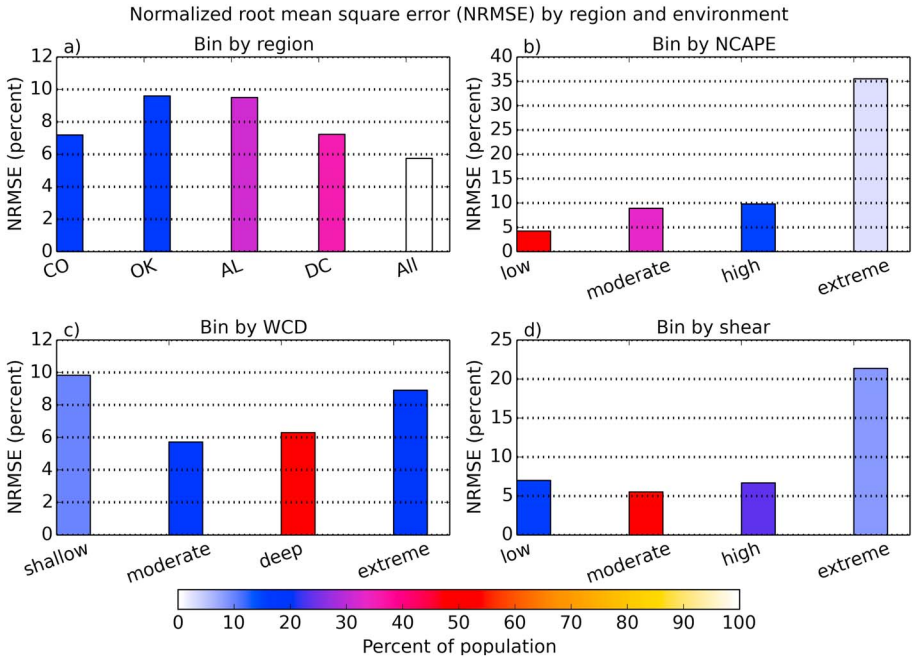

Figure 9. Bar plots of normalized root mean square error (NRMSE) for the VOL35 scheme when tested against observed flash rates for the 4322 thunderstorm cell data set described in section 2.7. NRMSE is shown as a function of (a) region (Colorado, Oklahoma, Alabama, and Washington, D.C.) and over all regions, (b) NCAPE, (c) WCD, and (d) surface-6 km vertical wind shear. All NRMSE quantities are given in percent. Low (shallow), moderate, high (deep), and extreme categories for the various environmental parameters are explained in Table 4. All regional and environmental bins are colored by their percent contribution to the total population of cells.

generally, normalized mean bias errors (not shown) were positive for all regional and environmental bins but always below +10% except for the extreme NCAPE bin, for which the bias error was +20.5%. This suggests that most cells produced lower flash rates than the 11 storms used to develop the VOL35 scheme. Although an attempt was made to sample a broad spectrum of DC3/CHILL-MIE storms, eight of the 11 storms sampled produced a mean flash rate >20 min^{-1} (Table 1). This sampling bias toward strongly electrified storms likely resulted in the overall positive bias of the VOL35 scheme. Larger errors in environments characterized by deeper WCDs are also expected (Figure 9c), since the VOL35 scheme was developed using data from Colorado storms with typically shallow WCDs. However, for all WCD bins, the average error remained below 10%. The extreme vertical wind shear category may be representative of strongly baroclinic environments with weak thermodynamic instability, possibly explaining the overestimation of flash rates (Figure 9d). Note, however, that the combined low/shallow and moderate (extreme) bins for NCAPE, WCD, and shear, respectively, contain 82% (3%), 28% (20%), and 68% (9%) of the 4322 total cells. The extreme environments in which the VOL35 errors are largest occurred rarely, suggesting this scheme can be applied with high confidence. The VOL35 scheme is therefore recommended for use in a wide variety of thunderstorm environments, although numerical modelers choosing to implement this scheme should be wary of the increasing errors in environments with extreme NCAPE.

When the performance of the VOL35 scheme is compared to the PR92CTH scheme for the NMQ data set, the VOL35 scheme performs much better *for high flash rate storms*. The error of the PR92CTH scheme, when calculated over all 4322 cells, is 7.2%, or only 1.4% worse than the VOL35 scheme. However, when testing of both schemes is limited to the 90th flash rate percentile (cells producing flash rates >33 min^{-1}), the PR92CTH scheme exhibits NRMSE of 23.4%, compared to 16.7% for the VOL35 scheme. More importantly, the normalized mean bias error of the PR92CTH was large and negative (−16.1%), compared to +4.0% for the VOL35 scheme. When tested for the 95th flash rate percentile (cells producing >81 flashes per minute), the negative PR92CTH bias is even larger (−30.1%), compared to +1.8% for the VOL35 scheme (NRMSE for the PR92CTH and VOL35 schemes were 35.8% and 21.0%, respectively).

The large negative biases of the PR92CTH scheme indicate this scheme's *inability to predict very high flash rates*. A storm producing 100 flashes per minute is likely no taller than a storm producing 10 flashes per minute. In order to produce significant lightning (multiple flashes per minute), both storms must become extensively vertically developed, exhibit deep convective updrafts, and likely extend to the tropopause. However, the 100 flashes per minute storm, based on the results herein, likely possesses greater mixed-phase 35 dB*Z* volume. While high flash rate storms are rare, they presumably produce large quantities of lightning NO_x and are thus of great interest to the LNO_x modeling community. In addition, if implemented into, for example, a superparameterized GCM, the PR92CTH scheme would predict a single maximum cloud-top height and would be ignorant of additional lightning activity in a grid box due to multiple simulated storms [*Romps et al.*, 2014]. In contrast, the VOL35 scheme would appropriately capture the additional lightning due to multiple simulated storm volumes. In this sense, the VOL35 scheme is a more physically realistic lightning parameterization.

5. Summary and Discussion

This study updated several flash rate parameterization schemes based on the relationship between total lightning flash rate and bulk storm parameters. The mixed-phase precipitating ice mass and 35 dB*Z* volume were confirmed to be reliable predictors of flash rate, but the coefficients of the relationships developed are specific to a sample of Colorado storms and differ from earlier studies. The mixed-phase 35 dB*Z* volume likely encloses the storm volume where most of the noninductive charging processes occur and hence was found to be a successful proxy for lightning flash rate. In contrast, indicators of updraft intensity such as W_{max} and updraft volume were less reliable predictors of flash rate, possibly because these parameters describe the properties of the main thunderstorm updraft and not the larger volume over which NIC processes and lightning discharges could occur. Cloud-top height [e.g., *Price and Rind*, 1992] was also found to strongly underestimate flash rate for high flash rate storms, as these storms were not anomalously tall and yet sometimes produced hundreds of flashes per minute. However, high flash rate storms were usually characterized by larger volumes of 35 dB*Z* than their low flash rate counterparts, indicative of the large quantities of ice necessary to sustain frequent lightning discharges.

Evidence that the simple VOL35 scheme successfully predicts flash rates for isolated storms in a variety of environments, including storms outside of Colorado, was also presented. The success of the VOL35 scheme

suggests that *reflectivity volume data may be sufficient to predict flash rate*, in place of more complex polarimetric or multiple-Doppler radar retrievals. In regions where dual-polarization radar observations are not widely available, the VOL35 scheme could be particularly useful. This scheme could also be tested on an even larger scale using a satellite radar reflectivity data set like GPM [*Smith et al.*, 2007], in conjunction with lightning data from the Geostationary Operational Environmental Satellite-R Series Geostationary Lightning Mapper [*Goodman et al.*, 2013], scheduled for launch in March 2016. This study is warranted in light of results like those of *Liu et al.* [2012], who found evidence of regional variability (e.g., differences for land versus oceanic convection) in the relationship of lightning to VOL35. Testing of the VOL35 scheme in this way is possible with the GPM precipitation radar, from which three-dimensional radar precipitation features (i.e., storm volumes) can be identified [*Smith et al.*, 2007]. Conversely, in remote regions lacking consistent radar observations, the VOL35 scheme could be inverted to diagnose thunderstorm reflectivity characteristics based on available lightning observations, analogous to the relationship between lightning and ice water content discussed by *Petersen et al.* [2005].

Ultimately, improved lightning flash rate parameterizations should be incorporated into lightning NO_x parameterization schemes in chemical transport models to further study lightning's impact on upper tropospheric chemistry and climate, although additional information besides flash rate (e.g., flash length) may be necessary to accurately simulate the lightning NO_x source. *Wang et al.* [1998] found that for a given peak current, NO_x production per unit discharge length was relatively constant for artificial laboratory sparks. The *Wang et al.* [1998] results suggest that the size of an individual lightning flash impacts the amount of NO_x it produces, so that the sum of all flash sizes in a storm may be related to storm total NO_x production. The LMA flash-counting algorithm provides a means to determine not only flash rate but also representative flash sizes (flash extents, section 2.6), and some studies have documented strong relationships between total flash rate and total flash extent (summed over all flashes) for individual storms [e.g., *Carey et al.*, 2014]. Other studies, such as *Bruning and MacGorman* [2013], have used LMA data to develop relationships between lightning flash rate and flash size and energy distributions. This work is essential to improve LNO_x parameterization schemes, and the present study provides strong motivation for its continuation. These studies, in conjunction with work that continues to test parameterizations like the VOL35 scheme on larger data sets, could make important progress toward reducing LNO_x uncertainty in models. Assessing the reliability of the VOL35 scheme over broad regions, such as the tropical oceans, would be an important step toward possibly implementing this scheme in a future convection-permitting regional or global model.

Acknowledgments

The authors wish to thank the following people who provided invaluable insight into this work, technical assistance, and many suggestions for improvement: W. Deierling, M. Barth, K. Pickering, K. Cummings, L. Carey, R. Mecikalski, E. Bruning, B. Dolan, P. Kennedy, and P. Hein. Colorado LMA data were provided by New Mexico Tech and are available at http://data.eol.ucar.edu/master_list/?project=DC3. CHILL and Pawnee radar data were provided by P. Kennedy of the CSU-CHILL national radar facility and are accessible at http://data.eol.ucar.edu/master_list/?project=DC3. Environmental sounding data were provided by the National Center for Atmospheric Research Earth Observing Laboratory (NCAR/EOL) under sponsorship of the National Science Foundation: http://data.eol.ucar.edu/. Environmental model analyses were provided by the National Climatic Data Center (NCDC). More information about the automated flash-counting algorithm can be found at https://github.com/deeplycloudy/lmatools. More information about the NMQ data is available at http://www.nssl.noaa.gov/projects/q2/. This study was supported by the National Science Foundation's Physical and Dynamical Meteorology (PDM) Program (grant AGS-1010657). The authors gratefully acknowledge the hard work and dedication of all participants of the DC3 field project.

References

Balakrishnan, N., and D. S. Zrnic (1990), Use of polarization to characterize precipitation and discriminate large hail, *J. Atmos. Sci.*, *47*(13), 1525–1540.

Barth, M. C., et al. (2014), The Deep Convective Clouds and Chemistry (DC3) field campaign, *Bull. Am. Meteorol. Soc.*, doi:10.1175/BAMS-D-13-00290.1.

Barthe, C., W. Deierling, and M. Barth (2010), Estimation of total lightning from various storm parameters: A cloud-resolving model study, *J. Geophys. Res.*, *115*, D24202, doi:10.1029/2010JD014405.

Blanchard, D. O. (1998), Assessing the vertical distribution of convective available potential energy, *Weather Forecasting*, *13*, 870–877.

Bringi, V. N., and V. Chandrasekar (2001), *Polarimetric Doppler Weather Radar: Principles and Applications*, Cambridge Univ. Press, Cambridge, U. K.

Bruning, E. C. (2013), *Streamed Clustering of Lightning Mapping Data in Python Using Sklearn*, vol. 2, Scientific Computing With Python (SciPy), Austin, Tex. [Available at http://www.youtube.com/watch?v=0Z17Q22HEMI, Accessed date 15 June 2015.]

Bruning, E. C., and D. R. MacGorman (2013), Theory and observations of controls on lightning flash size spectra, *J. Atmos. Sci.*, *70*, 4012–4029.

Calhoun, K. M., D. R. MacGorman, C. L. Ziegler, and M. I. Biggerstaff (2013), Evolution of lightning activity and storm charge relative to dual-Doppler analysis of a high-precipitation supercell storm, *Mon. Weather Rev.*, *141*, 2199–2223.

Carey, L. D., and S. A. Rutledge (1996), A multiparameter radar case study of the microphysical and kinematic evolution of a lightning producing storm, *Meteorol. Atmos. Phys.*, *59*, 33–64.

Carey, L. D., A. L. Bain, and R. Matthee (2014), Kinematic and microphysical control of lightning in multicell convection over Alabama during DC3, paper presented at 23rd International Lightning Detection Conference/5th International Lightning Meteorology Conference, Intl. Lightning Meteorolog. Conf., Tucson, Ariz., 18–21 March.

Cummings, K. A., T. L. Huntemann, K. E. Pickering, M. C. Barth, W. C. Skamarock, H. Holler, H.-D. Betz, A. Volz-Thomas, and H. Schlager (2013), Cloud-resolving chemistry simulation of a Hector thunderstorm, *Atmos. Chem. Phys.*, *13*, 2757–2777.

DeCaria, A. J., K. E. Pickering, G. L. Stenchikov, and L. E. Ott (2005), Lightning generated NO_x and its impact on tropospheric ozone production: A three-dimensional modeling study of a Stratosphere-Troposphere Experiment: Radiation, Aerosols, and Ozone (STERAO-A) thunderstorm, *J. Geophys. Res.*, *110*, D14303, doi:10.1029/2004JD005556.

Deierling, W. (2006), The relationship between total lightning and ice fluxes, PhD dissertation, 194 pp., Dep. of Atmos, Sci., Univ. of Alabama, Huntsville, Alabama.

Deierling, W., and W. A. Petersen (2008), Total lightning activity as an indicator of updraft characteristics, *J. Geophys. Res.*, *113*, D16210, doi:10.1029/2007JD009598.

Deierling, W., J. Latham, W. A. Petersen, S. M. Ellis, and H. J. Christian (2005), On the relationship of thunderstorm ice hydrometeor characteristics and total lightning measurements, *Atmos. Res.*, *76*(1–4), 114–126.

Deierling, W., W. A. Petersen, J. Latham, S. Ellis, and H. J. Christian (2008), The relationship between lightning activity and ice fluxes in thunderstorms, *J. Geophys. Res.*, *113*, D15210, doi:10.1029/2007JD009700.

Dolan, B., and S. A. Rutledge (2009), A theory-based hydrometeor identification algorithm for X-band polarimetric radars, *J. Atmos. Oceanic Technol.*, *26*, 2071–2088.

Dolan, B., S. A. Rutledge, S. Lim, V. Chandrasekar, and M. Thurai (2013), A robust C-band hydrometeor identification algorithm and application to a long-term polarimetric radar dataset, *J. Appl. Meteor. Climatol.*, *52*, 2162–2186.

Dye, J. E., et al. (2000), An overview of the Stratospheric-Tropospheric Experiment: Radiation, Aerosols, and Ozone (STERAO)-Deep Convection experiment with results for the July 10, 1996 storm, *J. Geophys. Res.*, *105*(D8), 10,023–10,045.

Ester, M., H.-P. Kriegel, J. Sander, and X. Xu (1996), A density-based algorithm for discovering clusters in large spatial datasets with noise, in *Proceedings of the Second International Conference on Knowledge Discovery and Data Mining (KDD-96)*, pp. 226–231, AAAI Press, Portland, Oregon.

Fehr, T., H. Holler, and H. Huntrieser (2004), Model study on production and transport of lightning-producted NO_x in a EULINOX supercell storm, *J. Geophys. Res.*, *109*, D09102, doi:10.1029/2003JD003935.

Finney, D. L., R. M. Doherty, O. Wild, H. Huntrieser, H. C. Pumphrey, and A. M. Blyth (2014), Using cloud ice flux to parameterise large-scale lightning, *Atmos. Chem. Phys.*, *14*, 12,665–12,682.

Fuchs, B. R., S. A. Rutledge, E. C. Bruning, J. R. Pierce, J. K. Kodros, T. J. Lang, D. MacGorman, P. Krehbiel, and W. Rison (2015a), Environmental controls on storm intensity and charge structure in multiple regions of the continental United States, *J. Geophys. Res. Atmos.*, *120*, 6575–6596, doi:10.1002/2015JD023271.

Fuchs, B. R., S. A. Rutledge, E. C. Bruning, P. Kennedy, and V. N. Bringi (2015b), Anomalously electrified storms in Colorado: A search for physical mechanisms, paper presented at 7th Conference on the Meteorological Applications of Lightning Data., Am. Meteorol. Soc., Phoenix, Ariz., 4–8 Jan.

Giangrande, S. E., S. Collis, J. Straka, A. Protat, C. Williams, and S. Krueger (2013), A summary of convective-core vertical velocity profiles using ARM UHF wind profilers in Oklahoma, *J. Appl. Meteorol. Climatol.*, *52*(10), 2278–2295.

Goodman, S. J., R. J. Blakeslee, W. J. Koshak, D. Mach, J. Bailey, D. Buechler, L. Carey, C. Schultz, M. Bateman, E. McCaul, and G. Stano (2013), The GOES-R Geostationary Lightning Mapper (GLM), *Atmos. Res.*, *125-126*, 34–49.

Heymsfield, A. J., and K. M. Miller (1988), Water vapor and ice mass transported into the anvils of CCOPE thunderstorms: Comparison with storm influx and rainout, *J. Atmos. Sci.*, *45*(22), 3501–3514.

Heymsfield, A. J., and A. G. Palmer (1986), Relationships for deriving thunderstorm anvil ice mass for CCOPE storm water budget estimates, *J. Clim. Appl. Meteor.*, *25*, 691–702.

Hubbert, J., and V. N. Bringi (1995), An iterative filtering technique for the analysis of copolar differential phase and dual-frequency radar measurements, *J. Atmos. Oceanic Technol.*, *12*, 643–648.

Jayaratne, E. R., C. P. R. Saunders, and J. Hallett (1983), Laboratory studies of the charging of soft-hail during ice crystal interactions, *Q. J. R. Meteorol. Soc.*, *109*, 609–630.

Lang, T. J., and S. A. Rutledge (2011), A framework for the statistical analysis of large radar and lightning datasets: Results from STEPS 2000, *Mon. Weather Rev.*, *139*, 2536–2551.

Liu, C., D. J. Cecil, E. J. Zipser, K. Fronfeld, and R. Robertson (2012), Relationships between lightning flash rates and radar reflectivity vertical structures in thunderstorms over the tropics and subptropics, *J. Geophys. Res.*, *117*, D06212, doi:10.1029/2011JD017123.

Liu, S. C., M. Trainer, F. C. Fehsenfeld, D. D. Parrish, E. J. Williams, D. W. Fahey, G. Hubler, and P. C. Murphy (1987), Ozone production in the rural troposphere and the implications for regional and global ozone distributions, *J. Geophys. Res.*, *92*(D4), 4191–4207.

MacGorman, D. R., et al. (2008), TELEX: The Thunderstorm Electrification and Lightning Experiment, *Bull. Am. Meteorol. Soc.*, *89*, 997–1013.

McCaul, E. W., S. J. Goodman, K. M. LaCasse, and D. J. Cecil (2009), Forecasting lightning threat using cloud-resolving model simulations, *Weather Forecasting*, *24*, 709–729.

Miller, L. J., C. G. Mohr, and A. J. Weinheimer (1986), The simple rectification to Cartesian space of folded radial velocities from Doppler radar sampling, *J. Atmos. Oceanic Technol.*, *3*, 162–174.

Mohr, C. G., and R. L. Vaughan (1979), An economical procedure for Cartesian interpolation and display of reflectivity factor data in three-dimensional space, *J. App. Meteorol.*, *18*, 661–670.

Mohr, C. G., L. J. Miller, R. L. Vaughan, and H. W. Frank (1986), The merger of mesoscale datasets into a common Cartesian format for efficient and systematic analyses, *J. Atmos. Oceanic Technol.*, *3*, 143–161.

Ott, L. E., K. E. Pickering, G. L. Stenchikov, D. J. Allen, A. J. DeCaria, B. Ridley, R.-F. Lin, S. Lang, and W.-K. Tao (2010), Production of lightning NO_x and its vertical distribution calculated from three-dimensional cloud-scale chemical transport model simulations, *J. Geophys. Res.*, *115*, D04301, doi:10.1029/2009JD011880.

Oye, D., and M. Case (1995), *REORDER: A Program for Gridding Radar Data — Installation and Use Manual for the UNIX Version*, Atmos. Technol. Div., Natl. Center for Atmos. Res., Boulder, Colo.

Oye, R., C. Mueller, and S. Smith (1995), Software for radar translation, visualization, editing, and interpolation, in *27th Conference on Radar Meteorology*, pp. 359–361, Am. Meteorol. Soc.

Petersen, W. A., H. J. Christian, and S. A. Rutledge (2005), TRMM observations of the global relationship between ice water content and lightning, *Geophys. Res. Lett.*, *32*, L14819, doi:10.1029/2005GL023236.

Pickering, K. E., A. M. Thompson, R. R. Dickerson, W. T. Luke, D. P. McNamara, J. P. Greenberg, and P. R. Zimmerman (1990), Model calculations of tropospheric ozone production potential following observed convective events, *J. Geophys. Res.*, *95*(D9), 14,049–14,062.

Pickering, K. E., Y. Wang, W.-K. Tao, C. Price, and J.-F. Muller (1998), Vertical distributions of lightning NO_x for use in regional and global chemical transport models, *J. Geophys. Res.*, *103*(D23), 31,203–31,216.

Potvin, C. K., K. L. Elmore, and S. J. Weiss (2010), Assessing the impacts of proximity sounding criteria on the climatology of significant tornado environments, *Weather Forecasting*, *25*, 921–930.

Price, C., and D. Rind (1992), A simple lightning parameterization for calculating global lightning distributions, *J. Geophys. Res.*, *97*(D9), 9919–9933.

Ray, P. S., C. L. Ziegler, and W. Bumgarner (1980), Single- and multiple-Doppler radar observations of tornadic storms, *Mon. Weather Rev.*, *108*, 1607–1625.

Reynolds, S. E., M. Brook, and M. F. Gourley (1957), Thunderstorm charge separation, *J. Meteorol.*, *14*, 426–436.

Rison, W., R. J. Thomas, P. R. Krehbiel, T. Hamlin, and J. Harlin (1999), A GPS-based three-dimensional lightning mapping system: Initial observations in central New Mexico, *Geophys. Res. Lett.*, *26*(23), 3573–3576.

Rison, W., P. R. Krehbiel, R. J. Thomas, D. Rodeheffer, and B. Fuchs (2012), The Colorado lightning mapping array, Abstract AE23B-0319 presented at 2012 Fall Meeting, AGU, San Francisco, Calif., 3–7 Dec.

Romps, D. M., J. T. Seeley, D. Vollaro, and J. Molinari (2014), Projected increase in lightning strikes in the United States due to global warming, *Science*, *346*(6211), 851–854.

Rowe, A. K., S. A. Rutledge, and T. J. Lang (2011), Investigation of microphysical processes occurring in isolated convection during NAME, *Mon. Weather Rev.*, *139*, 424–443.

Saunders, C. P. R., W. D. Keith, and R. P. Mitzeva (1991), The effect of liquid water on thunderstorm charging, *J. Geophys. Res.*, *96*(D6), 11,007–11,017.

Saunders, C. P. R., H. Bax-Norman, C. Emersic, E. E. Avila, and N. E. Castellano (2006), Laboratory studies of the effect of cloud conditions on graupel/crystal charge transfer in thunderstorm electrification, *Q. J. R. Meteorol. Soc.*, *132*, 2653–2673.

Schumann, U., and H. Huntrieser (2007), The global lightning-induced nitrogen oxides source, *Atmos. Chem. Phys.*, *7*, 3823–3907.

Seliga, T. A., and V. N. Bringi (1976), Potential use of radar differential reflectivity measurements at orthogonal polarizations for measuring precipitation, *J. Appl. Meteorol.*, *15*, 69–76.

Smith, E. A., et al. (2007), International Global Precipitation Measurement (GPM) program and mission: An overview, in *Measuring Precipitation From Space*, edited by V. Levizzani, P. Bauer, and F. J. Turk, Springer, Netherlands.

Takahashi, T. (1978), Riming electrification as a charge generation mechanism in thunderstorms, *J. Atmos. Sci.*, *35*(8), 1536–1548.

Thomas, R. J., P. R. Krehbiel, W. Rison, J. Harlin, T. Hamlin, and N. Campbell (2003), The LMA flash algorithm, in *Proceedings of the 12th International Conference on Atmospheric Electricity*, Int. Commission on Atmos. Electricity, 655–656.

Thomas, R. J., P. R. Krehbiel, W. Rison, S. J. Hunyady, W. P. Winn, T. Hamlin, and J. Harlin (2004), Accuracy of the lightning mapping array, *J. Geophys. Res.*, *109*, D14207, doi:10.1029/2004JD004549.

Tost, H., P. Jockel, and J. Lelieveld (2007), Lightning and convection parameterisations—Uncertainties in global modelling, *Atmos. Chem. Phys.*, *7*, 4553–4568.

Toumi, R., J. D. Haigh, and K. S. Law (1996), A tropospheric ozone-lightning climate feedback, *Geophys. Res. Lett.*, *23*(9), 1037–1040.

Wang, Y., and V. Chandrasekar (2009), Algorithm for estimation of the specific differential phase, *J. Atmos. Oceanic Technol.*, *26*, 2565–2578.

Wang, Y., A. W. DeSilva, and G. C. Goldenbaum (1998), Nitric oxide production by simulated lightning: Dependence on current, energy, and pressure, *J. Geophys. Res.*, *103*(D15), 19,149–19,159.

Wiens, K. C., S. A. Rutledge, and S. A. Tessendorf (2005), The 29 June 2000 supercell observed during STEPS. Part II: Lightning and charge structure, *J. Atmos. Sci.*, *62*(12), 4151–4177.

Williams, E. R. (1994), Global circuit response to seasonal variations in global surface air temperature, *Mon. Weather Rev.*, *122*, 1917–1929.

Williams, E. R., R. Zhang, and J. Rydock (1991), Mixed-phase microphysics and cloud electrification, *J. Atmos. Sci.*, *48*(19), 2195–2203.

Williams, E. R., V. Mushtak, D. Rosenfeld, S. Goodman, and D. Boccippio (2005), Thermodynamic conditions favorable to superlative thunderstorm updraft, mixed phase microphysics and lightning flash rate, *Atmos. Res.*, *76*, 288–306.

Zhang, J., et al. (2011), National Mosaic and Multi-Sensor QPE (NMQ) system: Description, results, and future plans, *Bull. Am. Meteorol. Soc.*, *92*, 1321–1338.